Microsyst Technol (2007) 13:97–101
DOI 10.1007/s00542-006-0259-z

TECHNICAL PAPER

# Power consumption analysis of surface acoustic wave sensor systems using ANSYS and PSPICE

**Yi Liu · Tianhong Cui**

Received: 29 June 2006 / Accepted: 23 August 2006 / Published online: 20 September 2006


**Abstract** The power consumption of a surface acoustic wave (SAW) sensor system was investigated using ANSYS and PSPICE. Simulation results show that several design parameters of the surface acoustic wave sensor, such as the center distance between two interdigital transducers (IDT), the thickness of the piezoelectric substrate, the finger space of the IDT, etc., can greatly affect the power consumption of the whole system. The results of this study will be helpful to optimum design and fabricate the SAW sensor systems with very low-power consumption.

## 1 Introduction

Surface acoustic wave (SAW) devices and technology started in 1965 with the concept of a thin metal interdigital transducer (IDT) on a polished piezoelectric plate, freeing elastic waves from their confinement in bulk material structures (White and Voltemer 1965). They were originally developed and are still primarily used as high-performance signal processing elements such as filters and delay lines for electronic systems and telecommunication areas (Campbell 1989). Despite this, SAW devices are also considered to be the earliest type of MEMS since they utilize mechanical (acoustic) waves, which are launched and detected electrically.

Y. Liu · T. Cui (✉)
Department of Mechanical Engineering,
University of Minnesota, 111 Church St SE,
Minneapolis, MN 55414, USA
e-mail: tcui@me.umn.edu

The basic type of surface acoustic wave was first discovered by Lord Rayleigh (1885), and hence the wave is also named as the Rayleigh wave. Surface acoustic wave has a longitudinal and a vertical shear component that can couple with a medium in contact with the device's surface. Such coupling strongly affects the amplitude and velocity of the wave and also enables SAW sensors to directly sense mass and mechanical properties. SAW has a velocity about five orders of magnitude less than the corresponding electromagnetic wave, which makes it among the slowest to propagate in solids. Since the Rayleigh wave has virtually all its acoustic energy confined within one wavelength of the surface, SAW sensors have the highest sensitivity among acoustic sensors (Drafts 2001).

The earliest reported SAW devices as microsensors were from Das et al. (1978) to measure pressure, and Wohltjen (1979) to measure thin-film chemical properties. These sensor applications resulted from the observed high sensitivity of SAW devices to external physical parameters and the properties of films deposited on the SAW substrate. Since then, the operation of SAW-based sensors has been widely demonstrated in many different applications, including gas and vapor concentrations (Bearzotti et al. 1992), ion concentrations in liquids (Caliendo et al. 1992), relative humidity (Caliendo et al. 1993), temperature (Hoummady and Hauden 1994), accelerations (Rokhlin et al. 1984), biosensor (Welsch et al. 1997), etc.

Finite element method (FEM) is a widely common technique to determine the surface acoustic wave properties of periodic structures. There are many publications about theoretical and practical results using FEM for SAW waveguide and transducer

(Koshiba et al. 1987; Yong et al. 1998; Smole et al. 2002). However, there are no FEM simulation results addressed for the power consumption of SAW sensors, which is a key feature of sensor systems that affect their applications. Low-power sensors are very important for the sensor integration. They may provide a new monitoring and control capability for a variety of applications in transportation, manufacturing, biomedical, environmental management, safety and security systems, etc.

In this paper, we demonstrate the simulation results of the power consumption of SAW sensor systems using the ANSYS and the PSPICE. This can help us to optimize the design and fabrication parameters in order to realize the very low-power consumption of the SAW sensor systems.

## 2 Theory and model

Piezoelectric effect is the coupling of structural and electrical fields, which is a natural property of materials such as quartz and ceramics. Applying a voltage to a piezoelectric material creates a displacement, and vibrating a piezoelectric material generates a voltage. The principle for piezoelectric effect can be summarized into the following equations:

$$\boldsymbol{T} = c\boldsymbol{S} - e\boldsymbol{E}, \tag{1}$$

$$\boldsymbol{D} = e^{T}\boldsymbol{S} + \varepsilon\boldsymbol{E}, \tag{2}$$

where $\boldsymbol{T}$ is the stress vector, $\boldsymbol{S}$ the strain vector, $\boldsymbol{D}$ the electric density flux vector, $\boldsymbol{E}$ the electric field vector, $c$ the elasticity matrix, $e$ the dielectric matrix, and $\varepsilon$ is the piezoelectric matrix. Equations 1 and 2 are the usual constitutive equations for structural and electrical fields, respectively, except for the coupling terms involving the piezoelectric matrix $e$. The matrices $c$, $e$, and $\varepsilon$ require knowledge of the piezoelectric material properties. Piezoelectric material ZnO is used for the simulation since it is suitable for monolithic fabrication and integration. Gold is used as the IDT material. The data of material properties data are obtained from several literatures (Qian et al. 1985; Van Zeijl et al. 1989).

To perform finite element analysis (FEA) involving piezoelectric effects requires coupled-field elements that take into account structural and electrical coupling. The coupled-field elements should contain all the necessary nodal degrees of freedom and include electrical–structural coupling in the element matrices. In the ANSYS simulation, we chose SOLID98 element to represent the piezoelectric substrate. The element has a quadratic displacement behavior and is well suited to model irregular meshes. When used in structural and piezoelectric analyses, SOLID98 has large deflection and stress stiffening capability. As to the gold electrodes, the 3D solid element SOLID186 is chosen to get more accurate result than SOLID185. SOLID186 has quadratic displacement behavior, and is also well suitable for modeling irregular meshes.

The structure of the 3D model for the SAW sensor is shown in Fig. 1, where $L$ is the center distance between two IDTs, $p$ is the space between two adjacent fingers (which is equivalent to half of the SAW wave length), and $t$ is the thickness of the piezoelectric substrate. Interdigital transducers are symmetrically placed on top of the piezoelectric substrate. The maximum acoustic-electric IDT interaction occurs at a characteristic frequency (working frequency) $f_0$ defined by:

$$f_0 = \frac{v}{\lambda_0} = \frac{v}{2p}, \tag{3}$$

where $\lambda_0$ is the working wavelength.

Our objective is to get the total power consumption for the SAW sensor system including the control circuit. The piezoelectric-circuit simulation in ANSYS can only employ simple passive components such as resistor, inductor, capacitor, etc., but not the active component like transistors. To get the total power consumption of the whole system, the PSPICE circuit simulation tool is applied to simulate the whole circuit including the SAW equivalent circuit and the control circuit. The equivalent circuit for SAW delay line based on coupling-of-mode theory by Nakamura is shown in Fig. 2 (Nakamura 1993).

In the 3D FEA of the SAW sensor, the top electrodes are glued to the bottom piezoelectric substrate.

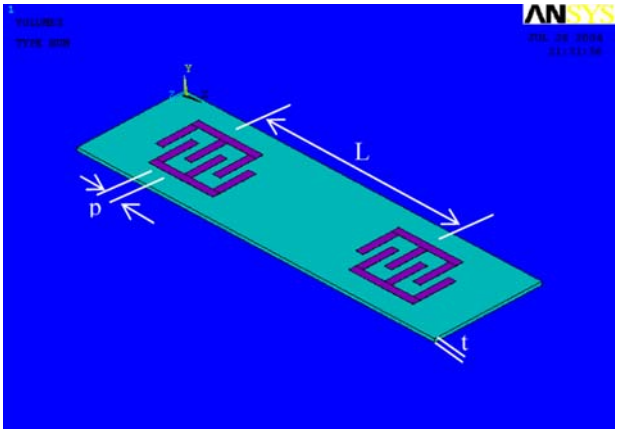


**Fig. 1** Structure of SAW sensor in ANSYS simulation

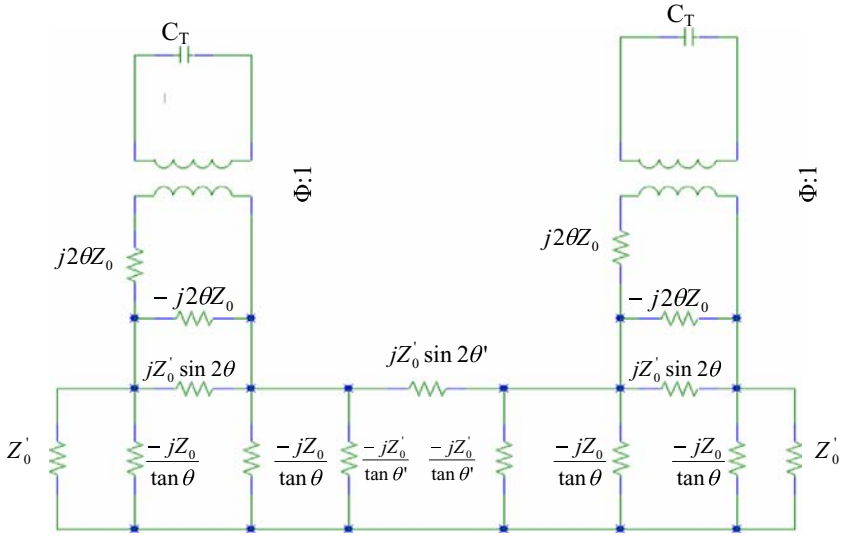


**Fig. 2** Equivalent circuit of the SAW delay line sensor (courtesy of Nakamura K.)

The sides of the piezoelectric substrate are fixed to meet the boundary condition. From the FEA piezoelectric coupled-field simulation, we can get the equivalent parameters, such as the capacitance, termination resistance, etc., for the SAW equivalent circuit. Next, combining the control circuit and the SAW delay line equivalent circuit into the PSPICE, we can obtain the total power consumption of the whole system.

## 3 Results and discussion

When using integration circuit (IC) fabrication technology, the power consumption of the control circuit part is very small. Hence, most of the power consumption for the whole sensor system results from the SAW sensor itself. We investigated the total power consumption affected by several design parameters, including the center distance between two IDTs, the piezoelectric substrate and the finger space (working frequency), etc.

### 3.1 Effect of the center distance on the power consumption

Figure 3 shows the total power consumption as a function of the center distance between two IDTs from 320 to 640 μm. The finger space is set as 40 μm, which means that the working wave length is 80 μm. From the figure, we can see that as the center distance increase, the total power consumption increase. The reason seems to be obvious: with increasing center distance, more power will lose during transporting from one IDT to another IDT, therefore more power consumption is needed to compensate the loss.

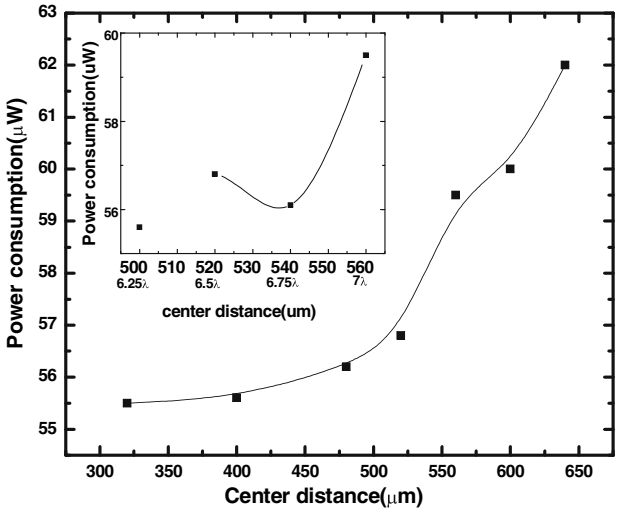


**Fig. 3** Power consumption versus the center distance between IDTs

From the inlet of Fig. 3, it can be seen that the power consumption changes alternatively with the period of half wavelength. Since the delay line performs like a resonator working at a resonant traveling wave (Benes et al. 1998), there is a chance to excite closely spaced alternative frequencies $f_n$ corresponding to another multiple of half wavelengths between the two IDTs,

$$n\frac{\lambda_n}{2} = n_0\frac{\lambda_0}{2} = l = n\frac{v}{2f_n} = n_0\frac{v}{2f_0}, \tag{4}$$

whereby the excitability decreases with increasing distance of $f_n$ from $f_0$. We can also see that within one

wavelength distance, the power consumption at distance of $n\lambda/4$ or $3n\lambda/4$ will be lower than that at $n\lambda/2$. To explain it, the schematic diagram of the wave transportation between two IDTs is shown in Fig. 4. When the center distance is $n\lambda/2$, the output IDT will meet the zero point of the transporting waves. On the other hand, when the center distance is $n\lambda/4$ or $3n\lambda/4$, the output IDT will meet the wave peaks, therefore more power is received. At the same power supply condition, smaller power is required at $n\lambda/4$ or $3n\lambda/4$ distance, resulting in lower power consumption.

### 3.2 Effect of the thickness of piezoelectric substrate on the power consumption

Figure 5 shows the thickness effect of piezoelectric substrates on the power consumption. When the thickness $t$ is $\lambda/4$, the power consumption reaches the minimum point. To explain it, the power carried by the SAW during transportation should be considered. The SAW follows the following rule during transportation (Datta 1986):

$$K^2 y_0 = \omega\varepsilon\kappa, \tag{5}$$

$$y_0 = \frac{2P}{A|\phi|^2}, \tag{6}$$

where $P$ is the power carried by a wave of amplitude $\Phi$ and cross-sectional area $A$, $K^2$ the piezoelectric coupling constant, $\omega$ the angular frequency, and $\varepsilon$ is the dielectric constant. From Eqs. 5 and 6, we can deduce the following equation for the power carried by SAW,

$$P = \frac{\omega\varepsilon\kappa A|\phi|^2}{2K^2}. \tag{7}$$

Surface waves propagate along the surface and decay into the depth within a distance in the order of a wavelength. It is thus not uniform in the $y$-direction. However, there is no variation in the transverse direction along the surface, that is, the wave is uniform in the $z$-direction. The particles move both in the direction of wave propagation ($x$) and perpendicular to the depth ($y$) so that the wave has a mixed compressional and shear character (Datta 1986). Figure 6 from Datta et al. (1986) shows the variation of particle displacement of $u_y$ and $u_x$ into the depth along a plane perpendicular to the propagation direction. Here, the particle displacement $u$ corresponds to wave amplitude $\Phi$ in Eq. 7. As shown in Fig. 6, the maximum wave amplitude occurs at the $1/4\lambda$ thickness due to the interference from the back surface. This corresponds to the maximum power carried by transportation during the SAW transportation, as shown by Eq. 7. Therefore, at the same power supply condition, the power loss during transportation is the lowest resulting in the minimum power consumption.

### 3.3 Effect of the finger space (working frequency) on the power consumption

Figure 7 shows the power consumption as a function of the finger space or the working frequency (inlet figure). When the finger space increases, the working distance decreases at the same time, as seen clearly in Eq. 3. From Fig. 7, we can see that the total power consumption decreases as the working frequency increases. This can

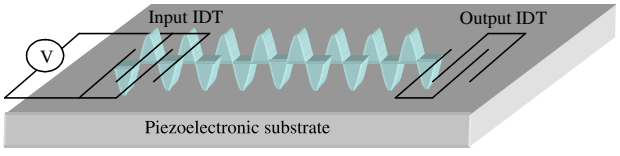


**Fig. 4** Wave transport between two IDTs of the SAW sensor

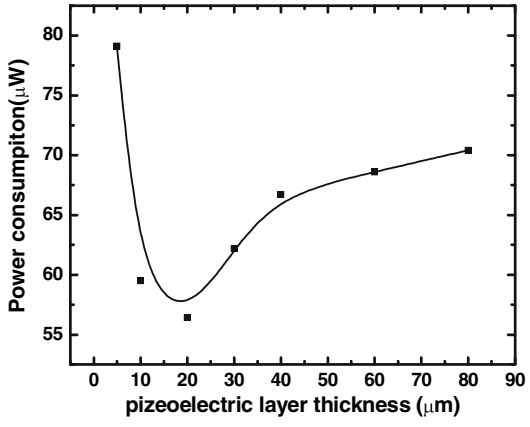


**Fig. 5** Power consumption with respect to the piezoelectric substrate

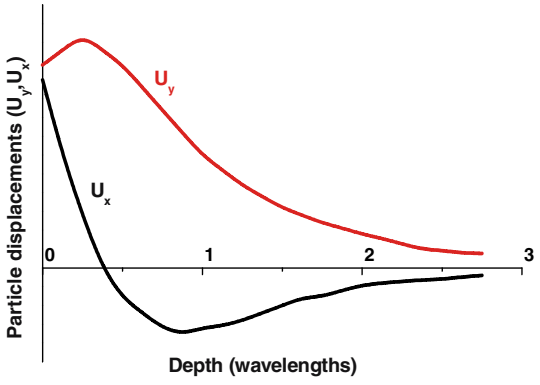


**Fig. 6** Variation of SAW particle displacement with depth

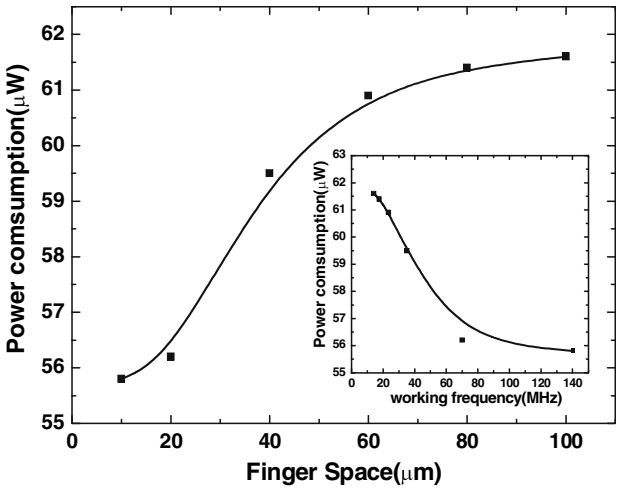


**Fig. 7** Power consumption versus the finger space or working frequency

also be explained by Eq. 7. The angular frequency $\omega$ is equal to $2\pi$ times of working frequency. At higher working frequency, the power carried by transporting SAW will also be larger, and hence the power transportation efficiency will be higher. Therefore, less power will lose during transportation, resulting in less power consumption.

## 4 Conclusion

The total power consumption of the SAW sensor and the control circuit was simulated using ANSYS and PSPICE. From the simulation results, we can see that the design parameters of SAW sensors will greatly affect the total power consumption. To obtain lower power consumption of the whole sensor system, several approaches can be considered:

(a) Reduce the center distance between the two IDTs of SAW sensor.
(b) Allow the center distance to be the $n/4$ times of the wavelength.
(c) Let the piezoelectric substrate be 1/4 of the wavelength.
(d) Reduce the distance between two adjacent fingers within the single IDT. This will depends on the resolution of the lithography fabrication technique.

Our research goal is to fabricate the monolithic integrated SAW sensor system with very low-power consumption. The simulation results would be very helpful to design the SAW sensor system and to optimize the corresponding fabrication process.

## References

Bearzotti A, Caliendo C, D'Amico A, Verona E (1992) Integrated optic sensor for the detection of $H_2$ concentrations. Sens Actuators B 7:685–688
Benes E, Groschl M, Seifert F, Pohl A (1998) Comparison between BAW and SAW sensor principles. IEEE Trans Ultrason Ferr 45:1314–1330
Caliendo C, D'Amico A, Mascini M, Moscone D, Verona E (1992) Acoustic love wave sensor for $K^+$ concentration in $H_2O$ solutions. Sens Actuators B 7:602–605
Caliendo C, D'Amico A, Furlani A, Iucci G, Russo MV, Verona E (1993) Surface acoustic wave humidity sensor. Sens Actuators B 16:288–292
Campbell C (1989) Surface acoustic wave devices and their signal processing applications. Academic press, Boston
Datta S (1986) Surface acoustic wave devices. Prentice-Hall, Englewood Cliffs, NJ
Drafts B (2001) Acoustic wave technology sensors. IEEE Trans Microw Theory 49:795–802
Das P, Lanzl C, Barone D (1978) A surface acoustic wave transmitting hydrophone. IEEE Ultrason Symp 458–463
Hoummady M, Hauden D (1994) Acoustic wave thermal sensitivity: temperature sensors and temperature compensation in microsensors. Sens Actuators A4:177–182
Nakamura K (1993) A simple equivalent circuit for interdigital transducers based on the coupled mode approach. IEEE Trans Ultrason Ferroelectr Freq Control 40:763–767
Koshiba M, Mitobe S, Suzuki M (1987) Finite-element solution of periodic waveguides for acoustic waves. IEEE Trans Ultrason Ferr 34:472–477
Qian Z, Zhang X, Zhao M, Xizhang W, Lin Y (1985) A modified ZnO film model for calculating elastic and piezoelectric properties. IEEE Trans Ultrason 32:630–633
Rayleigh L (1885) On waves propagating along the plane surface of an elastic solid. Proc Lond Math Soc 17:4–11
Rokhlin SI, Kornblit L, Gorodetsky G (1984) Surface acoustic wave pressure transducers and accelerometers. Prog Aerosp Sci 21:1–31
Smole P, Ruile W, Peter P (2002) Characterization of surface acoustic wave propagation in a ZnO layer on a conducting substrate. IEEE Ultrason Symp 1:307–310
Van zeijl PTM, Visser JH, Nanver LK (1989) FM radio receiver front-end circuitry with on-chip SAW filters. IEEE Trans Consum Electron 35:512–519
Welsch W, Klein C, Oksuzoglu M, Schickfus M, Hunklinger S (1997) Immunosensing with surface acoustic wave sensors. Sens Actuators A 62:562–564
White RM, Voltemer FW (1965) Direct piezoelectric coupling to surface elastic waves. Appl Phys Lett 17:314–316
Wohltjen H (1979) Surface acoustic wave probe for chemical analysis. Anal Chem 51:1458–1475
Yong YK, Garon R, Kanna S, Hashimoto KY (1998) Effects of periodically missing fingers and periodically shifted fingers on SAW propagation in quartz resonators. IEEE Int Freq Control Symp 461–469